

Evaluation of model-simulated source contributions to tropospheric ozone with aircraft observations in the factor-projected space

C. Shim^{1,*}, Y. Wang¹, and Y. Yoshida^{2,**}

¹Department of Earth and Atmospheric Sciences, Georgia Institute of Technology, 311 Ferst Drive, Atlanta, GA 30332, USA

²Goddard Earth Science & Technology Center, University of Maryland, Baltimore County, Baltimore, MD 21228, USA

* now at: Jet Propulsion Laboratory, California Institute of Technology, 4800 Oak Grove Drive Pasadena, CA 91109, USA

** now at: Atmospheric Chemistry and Dynamics Branch, NASA Goddard Space Flight Center, Greenbelt, MD 20771, USA

Received: 4 October 2007 – Published in Atmos. Chem. Phys. Discuss.: 2 November 2007

Revised: 7 February 2008 – Accepted: 29 February 2008 – Published: 26 March 2008

Abstract. Trace gas measurements of TOPSE and TRACE-P experiments and corresponding global GEOS-Chem model simulations are analyzed with the Positive Matrix Factorization (PMF) method for model evaluation purposes. Specially, we evaluate the model simulated contributions to O₃ variability from stratospheric transport, intercontinental transport, and production from urban/industry and biomass burning/biogenic sources. We select a suite of relatively long-lived tracers, including 7 chemicals (O₃, NO_y, PAN, CO, C₃H₈, CH₃Cl, and ⁷Be) and 1 dynamic tracer (potential temperature). The largest discrepancy is found in the stratospheric contribution to ⁷Be. The model underestimates this contribution by a factor of 2–3, corresponding well to a reduction of ⁷Be source by the same magnitude in the default setup of the standard GEOS-Chem model. In contrast, we find that the simulated O₃ contributions from stratospheric transport are in reasonable agreement with those derived from the measurements. However, the springtime increasing trend over North America derived from the measurements are largely underestimated in the model, indicating that the magnitude of simulated stratospheric O₃ source is reasonable but the temporal distribution needs improvement. The simulated O₃ contributions from long-range transport and production from urban/industry and biomass burning/biogenic emissions are also in reasonable agreement with those derived from the measurements, although significant discrepancies are found for some regions.

1 Introduction

Tropospheric O₃ has important environmental consequences. Photolysis of O₃ and the subsequent reaction of O(¹D) with water vapor (H₂O) in troposphere produces the hydroxyl radical (OH), which is the most important oxidant in troposphere. This tropospheric oxidation by OH determines the lifetime of major greenhouse gases such as methane (CH₄). The sources of tropospheric O₃ include photochemical production within the troposphere and transport from the stratosphere. Many studies have investigated the main sources to tropospheric O₃. Springtime O₃ increase is attributed to photochemical production (e.g., Penkett and Brice, 1986 and Liu et al., 1987). A number of studies using 3-D chemical transport models have focused on the effect of intercontinental transport on tropospheric O₃ concentrations from Asia to North America (e.g., Berntsen et al., 1999; Jaffe et al., 1999; Jacob et al., 1999; Bey et al., 2001). The effect of trans-Pacific transport is particularly noticeable in the spring (e.g., Jacob et al., 1999; Mauzerall et al., 2000; Wild and Akimoto, 2001; Tanimoto et al., 2002; Wang et al., 1998, 2006). On the other hand, the studies based on the observed correlations between O₃ and ⁷Be attributed this trend to transport of stratospheric O₃ (e.g., Oltmans and Levy, 1992; Dibb et al., 1994).

The observed relationships between tropospheric O₃ and CO provide additional diagnosis of O₃ sources (e.g., Fishman and Seiler, 1983; Chameides et al., 1987; Parrish et al., 1993). Furthermore, those relationships between simulated CO and O₃ offer a reasonable way to evaluate model simulations of O₃ (e.g., Chin et al., 1994). However, direct attribution of O₃ sources based on atmospheric measurements is



Correspondence to: C. Shim
(cshim@jpl.nasa.gov)

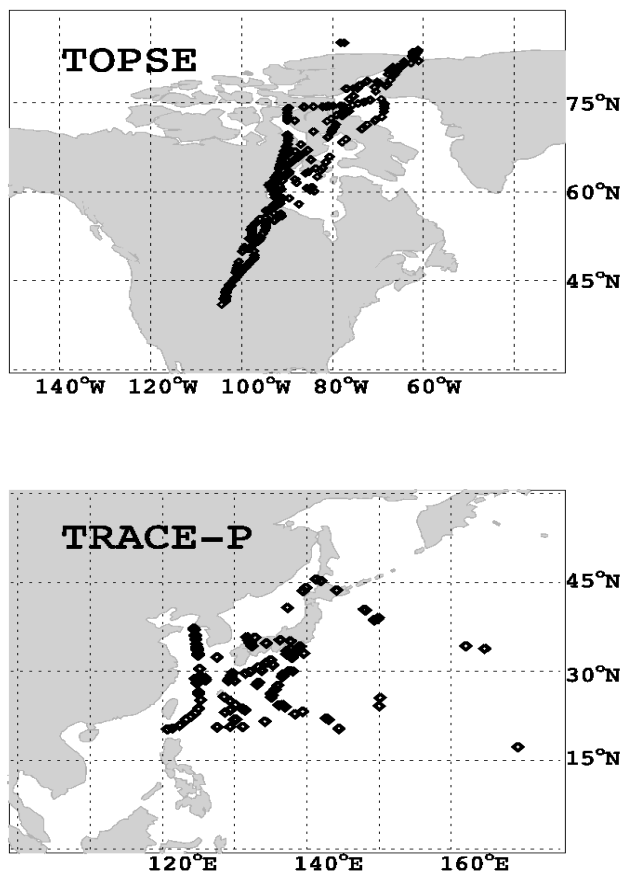


Fig. 1. Locations of aircraft measurements used in this study (after filtering).

difficult since tropospheric O₃ is a secondary product from primary emissions of trace gases. One method we used previously to diagnose sources of tropospheric trace gases is the positive matrix factorization (PMF) method, an advanced multi-variant factor analysis (Wang et al., 2003b; Shim et al., 2007). PMF analysis of the measurements obtained during the Tropospheric Ozone Production about the Spring Equinox (TOPSE) experiment found that the increasing seasonal trend of springtime O₃ at northern mid and high latitudes is attributed more to tropospheric O₃ production and transport, even though O₃ transport from the stratosphere is the largest contributor to O₃ variability (Wang et al., 2003b).

The factor attributions based on atmospheric measurements provide additional constraints on model simulated tropospheric O₃ sources beyond those provided by direct comparisons of simulated and observed trace gas concentrations. In this work, we apply the PMF method to the simulation results of a global 3-D chemical transport model (GEOS-Chem). As such, we can compare the PMF results to model simulations and evaluate the performance of GEOS-Chem on the basis of aircraft measurements. A main issue is how model simulated factor contributions to O₃ variability com-

pare with those based on the measurements. Unlike direct comparisons between observed and simulated trace gases, measurements and corresponding model results are first projected with PMF onto the factor space before model evaluation. In the factor space, a suite of chemicals can be evaluated simultaneously in a consistent and objective manner, which is difficult to achieve using direct comparisons between the measurements and model results. Aircraft measurements from two aircraft field campaigns, TOPSE and TRANsport of Chemical Evolution over the Pacific (TRACE-P, March–April 2001) experiments are used. We describe data selections from TOPSE and TRACE-P and GEOS-Chem simulations in Sect. 2.1. The PMF method is explained in Sect. 2.2. Evaluation of model results in the projected factor space is discussed in Sect. 3. Conclusions are given in Sect. 4.

2 Methodology

2.1 Measurements and GEOS-Chem simulations

Figure 1 shows the measurement regions during TOPSE and TRACE-P. The TOPSE experiment (February–May 2000) was conducted to investigate the photochemical transition during spring at northern mid and high latitudes (Atlas et al., 2003). The TRACE-P experiment (March–April 2001) was conducted to investigate the Asian outflow to the Pacific (Jacob et al., 2003). Both experiments took place during spring when significant transport of O₃ from the stratosphere is expected (e.g., Wang et al., 1998b and references therein)

In this study, we analyze relatively long-lived chemical tracers including O₃, total reactive nitrogen (NO_y), peroxyacetyl nitrate (PAN), CO, C₃H₈, CH₃Cl, and Beryllium-7 (⁷Be) and one dynamic tracer (potential temperature). Those tracers other than O₃ generally have specific primary source characteristics. NO_y is a good tracer for air masses influenced by tropospheric NO_x emissions (mostly from fossil fuel combustion, biomass burning, and soils) or transport from the stratosphere. PAN is produced only in the troposphere during oxidation of >C₂ hydrocarbons and its lifetime increases rapidly with increasing altitude. Therefore, it is a good tracer for photochemically aged air masses in the free troposphere. CO is for combustion influence primarily from fossil fuel, biofuel, and biomass and C₃H₈ is a good liquefied petroleum gas (LPG) tracer. CH₃Cl has its major sources from terrestrial biosphere and biomass burning (Yoshida et al., 2004, 2006). ⁷Be is produced mainly by cosmic rays in the stratosphere and upper troposphere and is generally used as a tracer for stratospheric air mass (Dibb et al., 2003). Potential temperature is a useful dynamic tracer since it is conserved in adiabatic processes. The analytical approach for the observed species is similar to the work by Wang et al. (2003b), but the number of chemicals used is smaller because only measured species that are also simulated by GEOS-Chem are selected. The resulting discrepancies with

the previous work by Wang et al. (2003b) will be discussed in Sect. 3.

Photochemical and dynamical environments vary dramatically with latitude. We separate the analysis regions to low, mid, and high latitudes. The TOPSE measurement data set is over mid (40–60° N, 87–104° W) and high latitudes (60–85° N, 61–94° W). We consider only coincident measurements, which are mostly limited by availability of ⁷Be measurements (144 coincident data points of all selected tracers for mid latitudes and 200 data points for high latitudes). Concentrations of O₃ in the selected subset have a similar probability distribution as the whole dataset, and the derived spring O₃ trends (TOPSE) of the subset are similar to the whole dataset. We exclude missing data because including large amounts of missing data (by assigning a large uncertainty to these data) would lead to a large underweight of the ⁷Be measurements and a loss of ⁷Be and O₃ correlation signal (Wang et al., 2003b). The ⁷Be and O₃ correlation is critical for analyzing the effect of stratospheric transport. The selected data have a bias towards high altitudes of 5–8 km (~70% of the data); therefore the evaluation results are more relevant for the middle and upper troposphere. The TRACE-P measurements data set is over mid latitudes (30–45° N, 125–240° E, 65 data points) and low latitudes (15–30° N, 120–205° E, 78 data points). The selected data also have a bias towards 7–12 km (40–50% of the data) due to the availability of ⁷Be measurements.

GEOS-Chem is a global 3-D chemical transport model driven by assimilated meteorological data from the Global Modeling Assimilation Office (GMAO) (Schubert et al., 1993). The 3-D meteorological fields are updated every six hours, and the surface fields and mixing depths are updated every three hours. We use version 7.24 with a horizontal resolution of 2° × 2.5° and 30 vertical layers (GEOS-3 meteorological fields were used). GEOS-Chem includes a comprehensive tropospheric O₃-NO_x-VOC chemical mechanism (Bey et al., 2001), which includes the oxidation mechanisms of 6 VOCs (ethane, propane, lumped >C₃ alkanes, lumped >C₂ alkenes, isoprene, and terpenes). Climatological monthly mean biomass burning emissions are from Duncan et al. (2003). The fossil fuel emissions are from the Global Emission Inventory Activity (GEIA) for other chemical compounds (Benkovitz et al., 1996; Olivier et al., 2001). The cross-tropopause O₃ transport from the stratosphere is simulated in the model using a passive ozone-like tracer (Synoz) (Mclinden et al., 2000). The annual net flux is ~475 Tg of O₃. For standard simulations, the model was first spun up for one year. The GEOS-Chem simulations for the selected five tracers and one dynamic tracer (O₃, NO_y, PAN, CO, C₃H₈, and potential temperature) are sampled at the same time and locations as the aircraft measurements. Simulated total reactive nitrogen (NO_y) is estimated by the sum of simulated NO_x, HNO₃ (nitric acid), HNO₄ (pernitric acid), PAN, and N₂O₅ (dinitrogen pentoxide).

We follow Liu et al. (2001 and 2004) in ⁷Be simulations. The ⁷Be source in GEOS-Chem is taken from the study by Lal and Peters (1967) as a function of altitude and latitude and ~70% of ⁷Be is emitted in the stratosphere. The seasonal and longitudinal dependence of ⁷Be productions is very small and not considered. The major sink of atmospheric ⁷Be is by wet deposition; the model considers scavenging in convective updrafts as well as first-order rainout and washout from both convective and large-scale precipitation (Liu et al., 2001). Liu et al. (2004) reduced the stratospheric ⁷Be source by a factor of 3. This simulation was first spun up for one year as well.

For model simulated CH₃Cl, we used the GEOS-Chem results by Yoshida et al. (2004). Contributions from the six sources (pseudo-biogenic, oceanic, biomass burning, incineration/industrial, salt marsh and wet land) are considered. The model results are evaluated extensively with surface and aircraft measurements; the model simulations are usually in good agreement with measurements in the northern hemisphere.

In order to investigate the stratospheric O₃ contributions in the model, we conducted tagged O₃ simulations to track the fractions of O₃ transported from the stratosphere (Liu et al., 2002). Photochemistry is considered in the simulations by taking archived O₃ production and loss rates from the GEOS-Chem standard simulations on a daily basis. In this manner, when projecting simulated O₃ variability in the factor space using PMF, we can examine the fractional contribution from the stratosphere as compared to tropospheric production (Sect. 3) in each factor.

2.2 PMF applications

The PMF method (Paatero and Tapper, 1994) explores factor categorization through the covariant structures of observed or simulated chemical and dynamical parameters (e.g., Paatero, 1997; Wang et al., 2003b; Liu et al., 2005). PMF generates only positive factor contributions, which enables a better physical interpretation of the results. In contrast, conventional the principal component analysis method lumps positively and negatively correlated tracers together. The data matrix **X** of *m* measurements by *n* tracers are decomposed in PMF analysis for *p* factors as

$$\mathbf{X} = \mathbf{GF} + \mathbf{E} \quad (1)$$

Or

$$x_{ij} = \sum_{k=1}^p g_{ik} f_{kj} + e_{ij} \quad (2)$$

$$i = 1, \dots, m; \quad j = 1, \dots, n; \quad k = 1, \dots, p.$$

where the *m* by *p* matrix **G** is the mass contributions of *k*th factor to *i*th sample (factor score), the *p* by *n* matrix **F** is the gravimetric average contributions of *k*th factor to *j*th chemical species (factor loadings), and the *m* by *n* matrix **E** is the

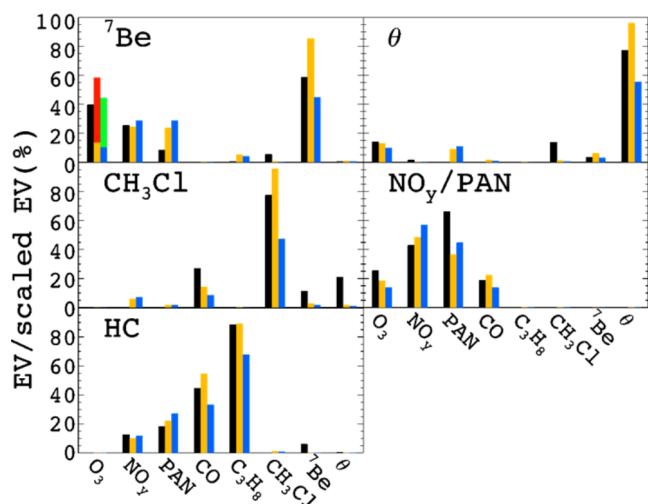


Fig. 2. Explained variation (% , defined in Sect. 2.2) profiles of the observed (shown in black) and simulated datasets (shown in yellow and red) at mid latitudes (40–60° N) during TOPSE. Also shown is the scaled EV profiles (in blue and green) for the simulated datasets for direct comparison with the measurements (Eq. 4, see text for details). The two-color bars for O₃ show the model simulated stratospheric (upper bar, red or green) and tropospheric (lower bar, yellow or blue) fractions. The results are for measurement data with O₃ concentrations <100 ppbv (and the corresponding model dataset).

error. In the PMF model, the solution is a weighted least squares fit, where the data uncertainties are used for determining the weights of the residuals in the error matrix. We also use the explained variation (EV),

$$EV_{kj} = \frac{\sum_{i=1}^m |g_{ik} f_{kj}|}{\left[\sum_{i=1}^m \left(\sum_{k=1}^p |g_{ik} f_{kj}| + |e_{ij}| \right) \right]} \quad (3)$$

to define the relative contributions of each factor to chemical species since the mixing ratios of different compounds are not directly comparable.

During PMF analysis, it is important to choose the number of factors that provide physically meaningful results. In this analysis, the order factor is determined by sorting the center-of-mass locations of the **G** or **F** matrix in ascending order. By evaluating the error matrix **E**, we define the range of mathematically acceptable number of factors (Paatero et al., 2002). We then inspect the factor profiles to choose the number of factors that gives the best physically meaningful results. In general, we pick as small a number of factors as possible to reduce the potential of overinterpreting of the dataset. Rotation is further used to improve factor separation (Paatero et al., 2002). However, the results presented in this work are insensitive to rotation.

As in the work by Wang et al. (2003b), the values of tracers are linearly scaled to a nondimensional range of 0–1 and assigned uniformly small uncertainty for the dataset. The scaling is applied because the chemical and dynamical trac-

ers have very different scales that affect the least square fitting in PMF. By scaling and assigning a uniform uncertainty, we assure that all tracers are weighted equally in the PMF analysis. In the analysis, we selected only coincident measurements of the selected tracers and corresponding model results. Missing measurement data are not used in order to reduce the uncertainty in the analysis. Following the procedure described above, PMF resolved 5 factors for TOPSE and 4 factors for TRACE-P in both observed and simulated datasets.

PMF was often used for source apportionments of surface aerosols (e.g., Lee et al., 1999). For that purpose, it is often necessary to assume that the composition of the air mass from a specific source does not change during transport. That assumption is unnecessary in this analysis since we evaluate how the simulated contributions to tropospheric ozone from different processes compare to the contributions derived from observations. Obviously the chemical characteristics of air masses are affected by transport. Our previous analyses (Wang et al., 2003b; Shim et al., 2007) indicate that although some collocated sources are mixed during transport, clear air mass separation based on the covariance of chemical and dynamical tracers can be obtained. We did not find evidence that transport and mixing “create” chemically distinct air mass.

3 Results and discussion

3.1 TOPSE

As mentioned in Sect. 2.1, the TOPSE results are biased toward the middle and upper troposphere. In order to capture the correlation between the stratospheric O₃ and ⁷Be using PMF, we have included the data points that have O₃ concentrations >100 ppbv (5% of the data set), which are generally associated with the lower stratospheric air. When analyzing the PMF results, however, we only use data points with O₃<100 ppbv to minimize the effect of these lower stratospheric data (Wang et al., 2003b). The simulated O₃ mixing ratios do not exceed 100 ppbv. We analyze the datasets for mid (40–60°) and high (60–85°) latitudes separately.

3.1.1 TOPSE at mid latitudes

PMF derived EV profiles from the observed and simulated datasets for TOPSE mid latitudes are shown in Fig. 2. Each factor is named after the tracers that show the largest variability (⁷Be, θ , CH₃Cl, NO_y/PAN, and hydrocarbons). The figure shows reasonably consistent factor profiles between observed and simulated datasets (black and yellow/red bars). Direct comparison of the EV profiles between the observed and simulated datasets can be misleading when the simulated variability differ significantly from the observations. For the simulated datasets, we therefore also show the scaled EV

Table 1. The factor scores correlations (r) with latitude, altitude, and C₂H₆/C₃H₈ for TOPSE mid latitudes.

Factors	Latitude		Altitude		C ₂ H ₆ /C ₃ H ₈	
	Obs	Mod	Obs	Mod	Obs	Mod
⁷ Be	-0.26	-0.37	0.42	0.62	0.02	0.1
θ	-0.59	-0.51	0.65	0.75	0.61	0.43
CH ₃ Cl	-0.34	-0.2	0.38	0.31	0.01	0.09
NO _y /PAN	0.32	0.32	-0.12	-0.1	-0.23	0.07
HC ¹	0.52	0.31	-0.65	-0.46	-0.64	-0.80

Extreme factor scores (outside 2 σ range) and the measurements that have O₃ greater than 100 ppbv are excluded ¹HC denotes the hydrocarbon factor.

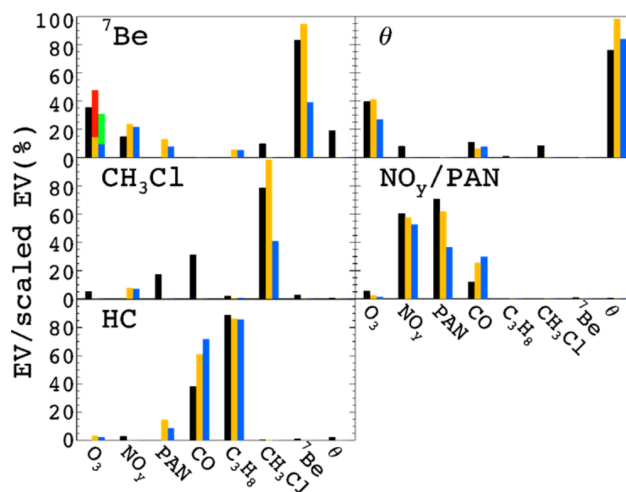
profiles (blue/green bars in Fig. 2–5) by the following equation,

$$EV_{kj}|_{\text{scaled}} = \frac{\left(\sum_{i=1}^m |g_{ik} f_{kj}| \right)_{\text{model}}}{\left[\sum_{i=1}^m \left(\sum_{k=1}^p |g_{ik} f_{kj}| + |e_{ij}| \right) \right]_{\text{measurements}}} \quad (4)$$

The ⁷Be factor in Fig. 2 shows the largest variability of ⁷Be for both observations and model (60% and 237 femtocurie per square centimeter (fCi/SCM) for the observations, 85% and 188 fCi/SCM for the model), indicating the stratospheric origin of the air masses. The stratospheric O₃ fraction from tagged O₃ simulation in this factor show ~75% of the stratospheric origin, and a small fraction of the tropospheric ⁷Be origin (~25%), due likely to upper tropospheric ⁷Be production, which is also evident in the small fractions of PAN in this factor. The ⁷Be factor is associated with the largest O₃ variability at mid latitudes (40% and 20 ppbv for the observations, 58% and 14 ppbv for the model). A notable underestimation in the simulated ⁷Be mean concentration is found (435 and 234 fCi/SCM for the observations and model, respectively). Including measured O₃ data >100 ppbv in the ⁷Be factor profile do not alter the results except a small decrease of the scaled EV of O₃. The same result is found for other regions, we therefore only show the profiles with measured O₃ ≤ 100 ppbv.

We examine the factor correlations with latitudes, altitude, and C₂H₆/C₃H₈ ratio in order to further investigate the factor characteristics (Table 1). The higher C₂H₆/C₃H₈ ratio reflects photochemically aged air masses (Wang and Zeng, 2004). The positive correlations of the ⁷Be factor with altitude ($r=0.42$ and 0.62 for the observed and simulated datasets, respectively) are expected for a factor dominated by transport from the stratosphere. The weak negative correlations with latitude indicate that stratosphere-troposphere exchange is likely more active at lower latitudes in 40–60° N region (Table 1).

The potential temperature (θ) factor has large variability of θ (Fig. 2). It explains 14% of observed O₃ vari-

**Fig. 3.** Same as Fig. 2, but for TOPSE high latitudes (60–85° N).

ability (3.6 ppbv) and 12.8% of simulated O₃ variability (3.1 ppbv). The negative factor correlations with latitude and CO ($r=-0.64$ and -0.52 , respectively, not shown in the table), and positive correlations with altitudes and C₂H₆/C₃H₈ ratio (Table 1) imply that this factor is likely associated with intercontinental long-range transport of O₃ from lower latitudes, which is consistent with the result by Wang et al. (2003b).

The CH₃Cl factor is characterized by large signals of CH₃Cl and no O₃ variability is explained by this factor (Fig. 2). This factor contains significant CO variability, which can imply the biomass burning influence. However, the very small factor correlations with C₂H₆/C₃H₈ ratio and negative correlation with latitude (Table 1) may support the large biogenic CH₃Cl emissions from the tropics (e.g., Yoshida et al., 2004, 2006) rather than biomass burning.

The NO_y/PAN factor has large signals of NO_y and PAN (Fig. 2) and this factor is the second important factor for tropospheric O₃ variability at mid latitudes (25.6% and 6.6 ppbv for the observations, 18.4% and 4.4 ppbv for the model). The positive correlation with latitude and much weaker correlations with altitude and C₂H₆/C₃H₈ ratio (Table 1) imply that the factor represents long-range transport of reactive nitrogen.

The hydrocarbon factor is characterized by large variability of CO and C₃H₈ (Fig. 2). There is no contribution to tropospheric O₃ variability. The positive correlation with latitude and clear negative correlations with altitudes and C₂H₆/C₃H₈ ratio reflect the influence of relatively fresh emissions from the surface (Table 1).

3.1.2 TOPSE at high latitudes

Five factors are identified for high latitudes (⁷Be, θ , CH₃Cl, NO_y/PAN, and hydrocarbons; Fig. 3). As mid latitudes, there is also significant difference in ⁷Be variability

Table 2. Same as Table 1, but for TOPSE high latitudes.

Factors	Latitude		Altitude		C ₂ H ₆ /C ₃ H ₈	
	Obs	Mod	Obs	Mod	Obs	Mod
⁷ Be	-0.08	-0.08	0.48	0.4	0.25	0.11
θ	-0.1	-0.2	0.51	0.55	0.22	0.4
CH ₃ Cl	-0.07	-0.2	0.38	0.46	0.18	-0.18
NO _y /PAN	0.16	0.07	0.02	-0.34	0.25	-0.14
HC ¹	-0.08	0.04	-0.43	-0.49	-0.77	-0.79

between observations and simulation (415 fCi/SCM and 206 fCi/SCM, respectively) in the ⁷Be factor, reflecting serious underestimation of ⁷Be by GEOS-Chem. Liu et al. (2001) artificially scaled down the stratospheric ⁷Be source by a factor of ~3 in order to adjust for some surface measurements of ⁷Be. However, the simulated ⁷Be mean concentrations and the variability accounted for in the ⁷Be factor show consistent underestimations by about a factor of 2 in TOPSE and TRACE-P (to be shown) datasets. It implies that the factor of 3 reduction in the stratospheric ⁷Be source in the standard GEOS-Chem model is too large.

The ⁷Be factor shows comparable O₃ variabilities between observations and simulation (34% and 13.7 ppbv for the observations, 45% and 12.4 ppbv for the model). The stratospheric O₃ fraction from the tagged O₃ simulation suggests that ~70% is of the stratospheric origin (Fig. 3). The tropospheric fraction for O₃ is ~30% in this factor. The positive correlations with altitude and negative correlations with CO support its stratospheric origin (Table 2).

The potential temperature (θ) factor shows large variabilities of θ (Fig. 3). Its contributions to O₃ levels are as much as that of the ⁷Be factor (39% and 15.4 ppbv for the observations, 41% and 10.7 ppbv for the model), which is different from mid latitudes. The positive correlation with altitude and C₂H₆/C₃H₈ ratio (Table 2) indicates that this factor is likely associated with transport of reactive-nitrogen poor air masses from lower latitudes. Tagged O₃ simulation shows that O₃ variability accounted for in this factor is produced in the troposphere (Fig. 3).

The CH₃Cl factor is characterized by large signals of CH₃Cl (78% and 38.6 pptv for the observations, 98% and 20.3 pptv for the model), but its contribution to O₃ variability is insignificant. This factor is positively correlated with altitude, consistent with long-range transport of high CH₃Cl air masses from lower latitudes since there are no significant sources of CH₃Cl at high latitudes.

The NO_y/PAN factor has large signals of NO_y and PAN (Fig. 3). This factor also has clear chemical signals of CO but not ⁷Be, implying that the air masses are influenced by industrial/fossil fuel emissions at high latitudes (Table 2). This factor, however, contributes to less than 5% of O₃ variability, reflecting the largely inactive photochemical environment at high latitudes in spring (Wang et al., 2003a).

Table 3. Factor contributions to O₃ seasonal increase (ppbv/month) for TOPSE.

Factors	Mid latitudes		High latitudes	
	Obs	Mod	Obs	Mod
⁷ Be	2.7	1.3	1.8	0.8
θ	0.3	0.4	1.2	0.8
CH ₃ Cl	0	0	0.3	0
NO _y /PAN	3.5	1.3	1.1	0.1
HC	0	0	0	-0.4
Total	6.5	3.0	4.3	1.3

Only the measurements O₃ < 100 ppbv are analyzed.

The hydrocarbon factor is characterized by a large variability of CO and C₃H₈ (Fig. 3). It does not contribute to tropospheric O₃ variability. Just as mid latitudes, the negative correlations with altitude and C₂H₆/C₃H₈ ratio reflect air masses affected by relatively fresh emissions (Table 2).

3.1.3 Springtime O₃ trends at northern mid and high latitudes

Understanding the contributions to the seasonal O₃ trend is another important purpose of this study. As stated in Sect. 2.1, this study analyzed only eight tracers due to the limited availability of simulated tracers, while the previous study (Wang et al., 2003b, hereafter referred to as the previous study) included fourteen tracers with seven factors. At mid latitudes, the seasonal increase of all factors of measurements is 6.48 ppbv/month (Table 3), consistent with the previous study (6.3 ppbv/month). The largest contributor to the O₃ seasonal trend is the NO_y/PAN factor (3.55 ppbv/month, Table 3) followed by the ⁷Be factor (2.66 ppbv/month). That is also consistent with the previous study (3.5 ppbv/month, and 2.5 ppbv/month, respectively). In contrast, the simulated overall seasonal increase is only 3.01 ppbv/month, indicating a large underestimation. The increase from the NO_y/PAN factor is underestimated (1.32 ppbv/month in the model), and the ⁷Be factor increase is also much smaller than that of observation (1.29 ppbv/month in the model).

At high latitudes, the overall springtime increase from the measurements is 4.29 ppbv/month (Table 3), comparable with the previous study (4.6 ppbv/month). In comparison, the simulated increase is only 1.3 ppbv/month, indicating a significant underestimation. The most contributions to the seasonal increases at high latitudes are from ⁷Be, θ , and NO_y/PAN factors (1.78, 1.16, and 1.10 ppbv/month, respectively) in the measurement dataset. In comparison, the corresponding trends in the model are much lower (0.76, 0.77, and 0.11 ppbv/month). The underestimation is particularly large for the NO_y/PAN factor, implying that simulated O₃ production in reactive-nitrogen rich air masses does not increase as

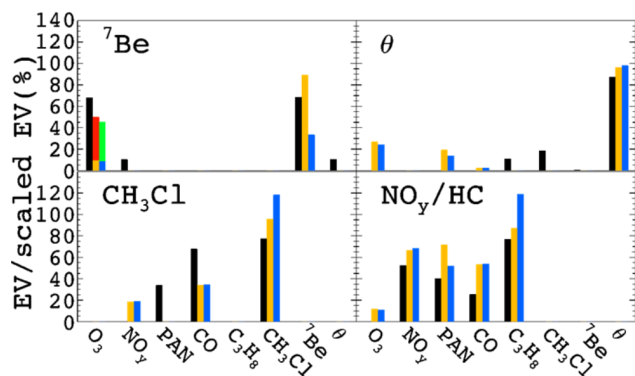


Fig. 4. Same as Fig. 2, but for TRACE-P mid latitudes (30–45° N).

much as in the observations. The negative O₃ trend in the hydrocarbon factor in the simulation but not in the measurements is a likely reflection of the problematic simulations of its major components (C₂H₆ and C₃H₈) in May by GEOS-Chem (Wang and Zeng, 2004).

The NO_y/PAN factor trend is consistent with the previous study. However, the contributions of ⁷Be and θ factors are different from those of the previous study (0.8 ppbv/month and 0.6 ppbv/month, respectively). The previous study had additional tracers resulting in the CH₄-halocarbon factor. It accounts for transport from lower latitudes, which contributes to the largest increase of O₃ at 1.7 ppbv/month at high latitudes. In this study, that large increase trend is apportioned into the ⁷Be and θ factors since we do not have CH₄ and halocarbon (other than CH₃Cl) simulations in GEOS-Chem. Because the PMF factor projections are for the same number of tracers, model results can still be evaluated in this analysis. The CH₄-halocarbon factor contribution to O₃ variability is, however, <10% (3 ppbv) at high latitudes in the previous study; thus the effect of the missing factor on factor apportioned O₃ variability is fairly insignificant in this study.

During TOPSE, the major contributions to the seasonal O₃ increase in springtime is from intercontinental transport of polluted air masses, while the major contributions to O₃ variability is from the stratospheric influences and long-range transport of O₃ from lower latitudes. While the model generally captures the factor contributions to O₃, factor contributions to the springtime increasing trend of O₃ in the measurements are severely underestimated. These model underestimations are also consistent with the results by Wang et al. (2006). Improvements in the seasonal transitions of cross-tropopause and intercontinental transport are needed in the model.

3.2 TRACE-P

The TRACE-P experiment was conducted to investigate the effects of Asian outflow to the Pacific during spring (Jacob et al., 2003). As mentioned in Sect. 2.1, the TRACE-P re-

Table 4. Same as Table 1, but for TRACE-P mid latitudes.

Factors	Latitude		Altitude		C ₂ H ₆ /C ₃ H ₈	
	Obs	Mod	Obs	Mod	Obs	Mod
⁷ Be	-0.37	0.05	0.12	0.63	0.32	0.28
θ	-0.33	-0.67	0.79	0.67	0.86	0.82
CH ₃ Cl	-0.02	0.11	-0.25	-0.77	-0.33	-0.6
NO _y /HC	0.18	-0.42	-0.77	-0.31	-0.64	-0.16

sults are biased toward the middle and upper troposphere (more than 40% of the data is above 7 km). Compared to TOPSE analysis, there are fewer coincident measurements limited mostly by the availability of ⁷Be measurements (65 and 79 for mid and low latitudes, respectively). We analyze the datasets for low (15–30°) and mid (30–45°) latitudes separately.

3.2.1 TRACE-P at mid latitudes

Four factors are identified for mid latitudes (⁷Be, θ , CH₃Cl, and NO_y/hydrocarbons, Fig. 4). The ⁷Be factor shows larger O₃ variability in the observations than model results (68% and 20.8 ppbv for the observations, 48.5% and 13.8 ppbv for the model). There is also a large underestimation in simulated ⁷Be variability (428 fCi/SCM and 211 fCi/SCM, respectively) for the reason discussed in Sect. 3.1.2. The tagged O₃ simulation shows that ~80% of O₃ variability in this factor is of the stratospheric origin (Fig. 4). While this factor in the simulated dataset showed a positive correlation with altitude ($r=0.63$), it has a much weaker correlation ($r=0.12$) in the measurements (Table 4). One possible reason for the large difference is that transport from the stratosphere occurs too close to TRACE-P regions in the model, resulting in stronger correlations. If the stratosphere-troposphere exchange occurs in regions farther away, further downward transport or mixing with low-altitude polluted air would reduce the gradients in altitude.

The potential temperature (θ) factor shows large signals of θ (Fig. 4). Positive correlations with altitudes and C₂H₆/C₃H₈ ratio in Table 4 characterize this factor as long-range transport of air masses from the tropics. While this factor accounts for 25.6% of O₃ variability in the simulated datasets, it has no contribution in the measurement dataset.

The CH₃Cl factor is characterized by the large signals of CH₃Cl and the contributions of this factor to O₃ variability are small in measured and simulated datasets (Fig. 4). The significant contributions to CO (Fig. 4) as well as negative correlations with altitude and C₂H₆/C₃H₈ ratio (Table 4), and the reactive nitrogen signals suggest a strong influence from biomass burning. This factor contributes to NO_y variability (168 pptv) only in the simulated dataset, and PAN variability (164 pptv) only in the observed dataset. Since PAN is an

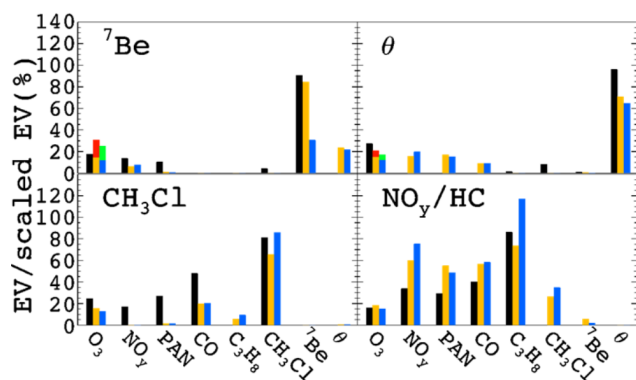


Fig. 5. Same as Fig. 2, but for TRACE-P low latitudes (15–30° N).

important component of NO_y, the signal in PAN will propagate to become a signal of NO_y. However, another large component of NO_y is HNO₃, which can be removed rapidly by wet deposition in the atmosphere. It appears to suggest that the scavenging of HNO₃ (a major component of NO_y) during transport and the production of PAN from biomass burning NO_x are underestimated by the model. The stronger negative correlation of the factor with altitude (Table 4) suggests that the altitude of biomass burning transport is lower in the model. This model bias also leads to a higher negative correlation with C₂H₆/C₃H₈ as is found here because mixing with locally emitted C₂H₆ and C₃H₈ tends to destroy the negative correlation (Table 4).

In TRACE-P analysis, the NO_y/PAN and hydrocarbon factors in TOPSE are combined (now NO_y/hydrocarbon factor) because the separation of those factors leads to incomparable factor profiles between the measurements and model results. The NO_y/hydrocarbon factor is characterized by a large variability of NO_y, PAN, CO, and C₃H₈ (Fig. 4). This factor shows a contribution to tropospheric O₃ variability only in the simulation (14.5%). This factor has negative correlations with altitudes and C₂H₆/C₃H₈ ratio, likely reflecting relatively the influence of fresh industrial/fossil fuel emissions over Asia (Table 4). The stronger negative correlations with C₂H₆/C₃H₈ ratio and altitude in the measurements than the simulations imply that mixing is too fast at low altitudes in the model.

3.2.2 TRACE-P at low latitudes

Four factors also are identified for low latitudes (⁷Be, θ , CH₃Cl, and NO_y/hydrocarbons, Fig. 5). The ⁷Be factor shows smaller O₃ variability in the measurements than the model simulation (17.4% and 7.1 ppbv for the observations, and 30.8 % and 9.9 ppbv for the model). Large underestimation by a factor of 3 is found in simulated ⁷Be variability (Fig. 5). There are no data with O₃ above 100 ppbv in both observations and simulation results at low latitudes. The stratospheric O₃ fraction from the tagged O₃ simulation

Table 5. Same as Table 1, but for TRACE-P low latitudes.

Factors	Latitude		Altitude		C ₂ H ₆ /C ₃ H ₈	
	Obs	Mod	Obs	Mod	Obs	Mod
⁷ Be	0.33	−0.06	0.39	0.67	0.06	0.41
θ	−0.05	0	0.98	0.93	0.61	0.52
CH ₃ Cl	0.22	0.4	0.03	0.13	−0.33	−0.4
NO _y /HC	0.25	0.35	−0.65	−0.53	−0.68	−0.75

shows that ~50% is due to transport from the stratosphere (Fig. 5), which is the smallest stratospheric influence among the datasets. The positive factor correlations with altitude reflect in part the contribution from the stratosphere (Table 5). The weaker correlations with altitude and C₂H₆/C₃H₈ ratio in the observed than simulated datasets likely reflect either a problem in the transport locations from the stratosphere or the mixing between stratospheric and tropospheric air masses in the model (Table 5).

The potential temperature (θ) factor shows large signals of θ (Fig. 5). While the ⁷Be factor is the largest contributor to simulated O₃ variability at low latitudes, the θ factor is the largest contributor to observed O₃ variability (27.4% and 11.1 ppbv for the observations, and 21% and 6.7 ppbv for the model). The model estimates a small stratospheric fraction of 15% in this factor. This factor contains small signals of simulated NO_y, PAN, and CO, which are absent in the observed dataset, indicating again that mixing of different air masses in the model is overestimated. The correlation coefficients are more consistent between observed and simulated datasets for this factor. The positive correlations with altitude and C₂H₆/C₃H₈ ratio (Table 5) and negative correlations with CO ($r=-0.66$ and -0.49 , not shown in the table) suggest the dominance of photochemically aged upper tropospheric air in this factor.

The CH₃Cl factor is characterized by large signals of CH₃Cl and a significant contribution to O₃ variability is found in this factor (24.6% and 9.9 ppbv for the observations, 15.7% and 5 ppbv for the model, Fig. 5). This factor contributes more to O₃ in the observations than the model. The larger contribution in the observations is associated with CO, NO_y, and PAN. In comparison, this factor in the simulated dataset has a smaller contribution from CO (22% and 17.4 ppbv) and negligible contributions from NO_y and PAN. The observed profile is consistent with the characteristics of biomass burning.

It appears that the contributions to PAN, NO_y, and CO from biomass burning are attributed to the NO_y/hydrocarbon factor in the model. Comparing the profiles between CH₃Cl and NO_y/hydrocarbon factors, a major separation factor between these factors is the correlation between C₃H₈ and CH₃Cl. In both datasets, almost all the C₃H₈ signals are in the NO_y/hydrocarbon factor. There is no correlation between

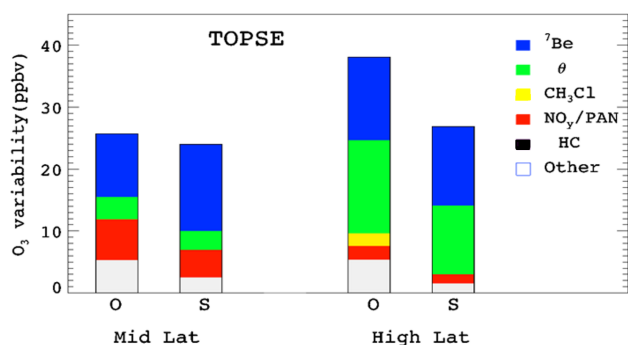


Fig. 6. O₃ variability ($[O_3]_{\text{average}} - [O_3]_{\text{min}}$) by factors for TOPSE. The two bars on the left are for mid latitudes and the two bars on the right are for high latitudes. “O” and “S” denote “observations” and “simulation”, respectively. “Other” denotes the unexplained fractions by PMF. “HC” denotes hydrocarbon.

C₃H₈ and CH₃Cl in the observed dataset. Consequently there is no CH₃Cl signal in the observed NO_y/hydrocarbon factor. The opposite is true in the simulated dataset, leading to a significant contribution to the CH₃Cl variability (29% and 17 pptv). The inadequate separation of C₃H₈ and CH₃Cl in the model may result from two sources. The first is that mixing is overestimated in the model, which results in excessive mixing of biomass burning and industrial/urban air masses. The second is that the locations of biomass burning or industrial/urban sources are misplaced in the model, which also leads to unrealistic mixing.

The NO_y/hydrocarbon factor is characterized by large variabilities of NO_y, PAN, CO, and C₃H₈ (Fig. 5). The factor contributions to these trace gases are lower in the observations than the model results because some of the enhancements in the model are due in part to biomass burning emissions. Interestingly, the factor contributions to tropospheric O₃ variability are comparable in the observations (16% and 6.5 ppbv) and model results (18.5% and 6 ppbv) even though the enhancements in NO_y, PAN, and CO are higher in the model results. The two datasets have comparable positive factor correlations with latitude, and large negative correlations with altitude and C₂H₆/C₃H₈ ratio indicating fresh pollution plumes from East Asia (Table 5).

4 Discussion and conclusions

Trace gas measurements of TOPSE and TRACE-P experiments and corresponding GEOS-Chem simulations are analyzed with the PMF method. The factor attributions based on the projections in the factor space allow a direct evaluation of model performance in simulating source contributions to tropospheric O₃ variability and its springtime increase (during TOPSE). We select a suite of relatively long-lived variables, which are available both in observations and GEOS-

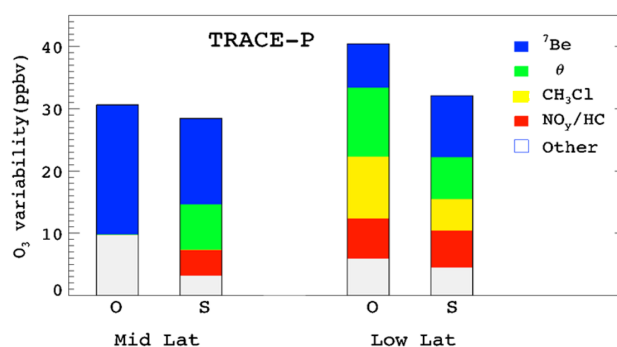


Fig. 7. Same as Fig. 6, but for TRACE-P. Two bars on the left are for mid latitudes and the two bars on the right for low latitudes.

Chem model: seven chemicals (O₃, NO_y, PAN, CO, C₃H₈, CH₃Cl, and ⁷Be) and one dynamic tracer (potential temperature). The evaluation has a bias towards a high altitude of 5–8 km (~70% of the data) for TOPSE and 7–12 km (~50% of the data) for TRACE-P, due to the availability of ⁷Be measurements.

In general, the factor loadings between the observations and simulations are in better agreement during the TOPSE experiment than TRACE-P. The former experiment took place in remote regions. Therefore, the model results are not as sensitive to source locations as for the latter experiment. There are also slightly more data points (determined largely by the availability of ⁷Be measurements) in the former experiment. We summarize the factor contributions to O₃ variability in Figs. 6 and 7.

The ⁷Be factor is found in all regions. Among all the factors, the largest discrepancy is found in the variability of ⁷Be, which is controlled largely by its source in the stratosphere. The simulated results are a factor of 2–3 lower than those observed. The large underestimation is due to the default reduction of the stratospheric ⁷Be source by a factor of ~3. Inadvertently, the default reduction provides a test for the PMF analysis.

Tagged O₃ simulations in the model indicate that the O₃ signal in the ⁷Be factor is controlled largely (70–80%) by transport from the stratosphere at mid and high latitudes. Only over the lower latitude does the stratospheric contribution drop to ~50%. The ⁷Be factor explains 34–40% of O₃ variability in the measurement dataset during TOPSE, in agreement with the simulated dataset. During TRACE-P, this factor contributes 68% and 17% at mid and low latitudes, respectively in the measurement dataset. In comparison, the contributions in the simulated datasets are also higher at mid latitudes (49%) and lower at low latitudes (31%). In general, we find that the decrease of stratospheric O₃ contributions (and the increase of tropospheric O₃ contributions) from mid to low latitudes during TRACE-P are much larger in the measured than simulated datasets. One potential reason is that

mixing is overestimated between mid and low latitudes in the model, reducing the gradients between the two latitude bands.

Another common factor is the θ factor. There are consistent positive correlations of this factor with altitude and C₂H₆/C₃H₈ ratio, indicating long-range transport in the upper troposphere. The contribution of this factor to reactive nitrogen is small, reflecting likely chemical processing during transport. The large contribution to O₃ variability at high latitudes during TOPSE (~40%) in the measurement dataset is in agreement with the simulated dataset. In comparison, its contributions to mid latitudes during TOPSE are much lower in both datasets. During TRACE-P, there is no contribution from this factor to O₃ variability in the measurement dataset at mid latitudes. However, 26% contribution is found in the simulated dataset. A similar situation is found for the NO_y/hydrocarbon factor. Excessive mixing between mid and low latitudes could explain some of the discrepancy. Further, the unresolved portion of O₃ variability is ~30% in this case, much higher than the range of 11–19% in the other cases. Some of the unresolved portion is due to O₃ production in the troposphere.

A third common factor found is the CH₃Cl factor. The contributions of this factor to O₃ are usually small. The exception is at low latitudes during TRACE-P, when biomass burning contributes to both CH₃Cl and O₃. Some of the biomass burning contribution in the simulated datasets is attributed to the NO_y/hydrocarbon factor since simulated C₃H₈ is correlated with CH₃Cl. The latter correlation was not found in the measurement dataset. Thus, we combine the CH₃Cl and NO_y/hydrocarbon factor contributions to O₃ variability; it is somewhat higher in the measurement dataset (41%) than the simulated dataset (34%). As discussed previously, the difference can be reduced if mixing is reduced between mid and low latitudes in the model.

During TOPSE, the NO_y/PAN factor is resolved separately from the hydrocarbon factor. The latter made no contribution to O₃ variability. The NO_y/PAN factor contributions are much higher at mid latitudes (18–26%) than high latitudes (<5%) in measured and simulated datasets, reflecting more active photochemistry at mid latitudes in spring.

Since the TOPSE experiment lasted longer than TRACE-P, we compared the factor contributions to the seasonal trend of O₃ in the observed and simulated datasets. Despite reasonably good agreements in the averaged contributions, the trends of factor contributions are quite different. The observed springtime O₃ increase is higher than simulated by a factor 2 at mid latitudes (6.5 vs. 3 ppbv/month) and a factor of 3 at high latitudes (4.3 vs. 1.3 ppbv/month). The increasing trend from the stratospheric contribution (the ⁷Be factor) is underestimated by a factor of 2. The increasing trend from the tropospheric contribution is simulated well for the θ factor. However, the increasing trend from O₃ production by reactive nitrogen (the NO_y/PAN factor) is underestimated by a factor of >3 (3.5 ppbv/month vs. 1.3 ppbv/month at mid

latitudes and 1 ppbv/month vs. 0.1 ppbv/month at high latitudes). These results suggest that more attention needs to be placed on improving the simulations of the temporal trends of trace gases in chemical transport models.

Acknowledgement. This work was supported by the National Science Foundation Atmospheric Chemistry Program. The GEOS-CHEM model is managed at Harvard University with support from the NASA Atmospheric Chemistry Modeling and Analysis Program.

Edited by: R. von Glasow

References

- Atlas, E. L., Ridley, B. A., and Cantrell, C.: Tropospheric Ozone Production about the Spring Equinox (TOPSE) Experiment: Introduction, *J. Geophys. Res.* 108(D4), 8353, doi:10.1029/2002JD003172, 2003.
- Benkovitz, C. M., Schwartz C. E., Jensen, M. P., et al.: Global gridded inventories of anthropogenic emissions for sulfur and nitrogen, *J. Geophys. Res.*, 101(D22), 29 239–29 253, 1996.
- Berntsen, T. K., Karlsdottir S., and Jaffe D. A.: Influence of Asian emissions on the composition of air reaching the northwestern United States, *Geophys. Res. Lett.*, 26, 2171–2174, 1999.
- Bey, I., Jacob, D. J., Yantosca, R. M., et al.: Global modeling of tropospheric chemistry with assimilated meteorology: Model description and evaluation, *J. Geophys. Res.*, 106, 23 073–23 096, 2001.
- Chameides, W. L., Davis, D. D., Rodgers, M. O., et al.: Net ozone photochemical production over the eastern and central north Pacific as inferred from CTE/CITE 1 observations during fall 1983, *J. Geophys. Res.*, 92, 2131–2152, 1987.
- Chen, P.: Isentropic cross-tropopause mass exchange in the extratropics, *J. Geophys. Res.*, 100, 16 661–16 673, 1995.
- Chin, M., Jacob, D. J., and Munger, J. W., et al.: Relationship of ozone and carbon monoxide over North America, *J. Geophys. Res.*, 99, 14 565–14 573, 1994.
- Dibb, J. E., Meeker, L. D., Finkel, R. C. J., et al.: Estimation of stratospheric input to the Arctic troposphere: ⁷Be and ¹⁰Be in aerosols at Alert, Canada, *J. Geophys. Res.*, 99, 12 855–12 864, 1994.
- Dibb, J. E., Talbot, R. W., Scheuer, E., et al.: Stratospheric influence on the northern North American free troposphere during TOPSE: ⁷Be as a stratospheric tracer, *J. Geophys. Res.*, 108(D4), 8363, doi:10.1029/2001JD001347, 2003.
- Duncan, B. N., Martin, R. V., Staudt, A. C., et al.: Interannual and seasonal variability of biomass burning emissions constrained by satellite observations, *J. Geophys. Res.*, 108(D2), 4100, doi:10.1029/2002JD002378, 2003.
- Fishman, J. and Seiler, W.: Correlative nature of ozone and carbon monoxide in the troposphere: Implications for the tropospheric ozone budget, *J. Geophys. Res.*, 88, 3662–3670, 1983.
- Holton, J. R., Haynes P. H., McInyre, E. M., et al.: Stratosphere-troposphere exchange, *Rev. Geophys.*, 33, 403–439, 1995.
- Jacob, D. J., Logan J. A., and Murti P. P.: Effect of rising Asian emissions on surface ozone in the United States, *Geophys. Res. Lett.*, 26, 2175–2178, 1999.

- Jacob, D. J., Crawford, J. H., Kleb, M. M., et al.: Transport and Chemical Evolution over the Pacific (TRACE-P) aircraft mission: Design, execution, and first results, *J. Geophys. Res.*, 108(D20), 1–19, 2003.
- Jaffe, D., Anderson, T., Covert, D., et al.: Transport of Asian air pollution to North America, *Geophys. Res. Lett.*, 26, 711–714, 1999.
- Lee, E., Chan, C. K., and Paatero, P.: Application of positive matrix factorization in source apportionment of particulate pollutants in Hong Kong, *Atmos. Environ.*, 33, 3201–3212, 1999.
- Liu, H., Jacob, D. J., Bey, I., and Yantosca, R. M.: Constraints from ²¹⁰Pb and ⁷Be on wet deposition and transport in a global three-dimensional chemical tracer model driven by assimilated meteorological fields, *J. Geophys. Res.*, 106, 12 109–12 128, 2001.
- Liu, H., Jacob, D. J., Chan, L. Y., et al.: Sources of tropospheric ozone along the Asian Pacific Rim: An analysis of ozonesonde observations, *J. Geophys. Res.*, 107(D21), 4573, doi:10.1029/2001JD002005, 2002.
- Liu, H., Jacob, D. J., Dibb, J. E., Fiore, A. M., et al.: Constraints on the sources of tropospheric ozone from ²¹⁰Pb-⁷Be-O₃ correlations, *J. Geophys. Res.*, 109, D07306, doi:10.1029/2003JD003988, 2004.
- Liu, S. C., Trainer, M., Fehsenfeld, F. C., et al.: Ozone production in the rural troposphere and the implications for regional and global ozone distributions, *J. Geophys. Res.*, 92, 4191–4207, 1987.
- Liu, W., Wang, Y., Russell, A., et al.: Atmospheric aerosols over two urban-rural pairs in southeastern United States: Chemical composition and sources, *Atmos. Environ.*, 39, 4453–4470, 2005.
- Logan, J. A.: Tropospheric ozone: Seasonal behavior, trends, and anthropogenic influence, *J. Geophys. Res.*, 90, 10 463–10 482, 1985.
- Mauzerall, D. L., Narita, D., Akimoto, H., et al.: Seasonal characteristics of tropospheric ozone production and mixing ratios over East Asia: A global three dimensional chemical transport model analysis, *J. Geophys. Res.*, 105, 17 895–17 910, 2000.
- McLinden, C. A., Olsen, S. C., and Hannegan, B., et al.: Stratospheric ozone in 3-D models: A simple chemistry and the cross-tropopause flux, *J. Geophys. Res.*, 105, 14 653–14 665, 2000.
- Olivier, J. G. J. and Berdowski, J. J. M.: Global emissions sources and sinks, in: *The Climate System*, edited by: Berdowski, J., Guicherit, R., and Heij, B. J., A. A. Balkema Publishers/Swets & Zeitlinger Publishers, Lisse, The Netherlands, ISBN 90-5809-255-0, 33–78, 2001.
- Oltmans, S. J. and Levy II, H.: Seasonal cycle of surface ozone over the western North Atlantic, *Nature*, 358, 392–394, 1992.
- Paatero, P. and Tapper, U.: Positive Matrix Factorization: a non-negative factor model with optimal utilization of error estimates of data values, *Environmetrics*, 5, 111–126, 1994.
- Paatero, P.: Least squares formulation of robust non-negative factor analysis, *Chemomet. Intell. Lab. Sys.*, 37, 23–35, 1997.
- Paatero, P., Hopke, P. K., Song, X.-H., et al.: Understanding and controlling rotations in factor analytic models, *Chemomet. Intell. Lab. Sys.*, 60, 253–264, 2002.
- Parrish, D. D., Holloway, J. S., Trainer, M., et al.: Export of North American ozone pollutions to the North Atlantic Ocean, *Science*, 259, 1436–1439, 1993.
- Penkett, S. A. and Brice K. A.: The spring maximum in photo-oxidants in the Northern Hemisphere troposphere, *Nature*, 319, 655–657, 1986.
- Shim, C., Wang, Y., Singh, H. B., et al.: Source characteristics of oxygenated volatile organic compounds and hydrogen cyanide, *J. Geophys. Res.*, 112, D10305, doi:10.1029/2006JD007543, 2007.
- Tanimoto, H., Wild, O., Kato, S., et al.: Seasonal cycles of ozone and oxidized nitrogen species in northeast Asia: 2. A model analysis of the roles of chemistry and transport, *J. Geophys. Res.*, 107(D23), 4706, doi:10.1029/2001JD001497, 2002.
- Wang, Y., Jacob, D. J., and Logan, J. A.: Global simulation of tropospheric O₃-NO_x-hydrocarbon chemistry, 3. origin of tropospheric ozone and effects of non-methane hydrocarbons, *J. Geophys. Res.*, 103, 10 757–10 767, 1998b.
- Wang, Y., Liu, S. C., Wine, P. H., et al.: Factors Controlling Tropospheric O₃, OH, NO_x, and SO₂ over the Tropical Pacific during PEM-Tropics B, *J. Geophys. Res.*, 106, 32 733–32 748, 2001.
- Wang, Y., Ridley, B., Fried, A., et al.: Springtime photochemistry at northern mid and high latitudes, *J. Geophys. Res.*, 108(D4), 8358, doi:10.1029/2002JD002227, 2003a.
- Wang, Y., Shim, C., Blake, N., et al.: Intercontinental transport of pollution manifested in the variability and seasonal trend of springtime O₃ at northern middle and high latitudes, *J. Geophys. Res.*, 108(D21), 4683, doi:10.1029/2003JD003592, 2003b.
- Wang, Y. and T. Zeng; On tracer correlations in the troposphere: The case of ethane and propane, *J. Geophys. Res.*, 109, D24306, doi:10.1029/2004JD005023, 2004.
- Wang, Y., Choi, Y. S., Zeng, T., et al.: Late-spring increase of trans-Pacific pollution transport in the upper troposphere, *Geophys. Res. Lett.*, 33, L01811, doi:10.1029/2005GL024975, 2006.
- Wild, O. and Akimoto, H.: Intercontinental transport of ozone and its precursors in a three-dimensional global CTM, *J. Geophys. Res.*, 106, 27 729–27 744, 2001.
- Yoshida, Y., Wang, Y. H., Zeng, T., et al.: A three-dimensional global model study of atmospheric methyl chloride budget and distributions, *J. Geophys. Res.*, 109, D24309, doi:10.1029/2004JD004951, 2004.